Analysis and optimization of light outcoupling in OLEDs with external hierarchical textures

Milan Kovačič,[1,*] (iD) **Dinara Samigullina,**[2] **Felix Bouchard,**[3] **Janez Krč,**[1] (iD) **Benjamin Lipovšek,**[1] **Marcos Soldera,**[3,4] **Andrés Fabián Lasagni,**[3,5] **Sebastian Reineke,**[2] **and Marko Topič**[1] (iD)

[1]*University of Ljubljana, Faculty of Electrical Engineering, Tržaška 25, 1000 Ljubljana, Slovenia*
[2]*Technische Universität Dresden, Dresden Integrated Center for Applied Physics and Photonic Materials (IAPP) and Institute for Applied Physics, Nöthnitzer Str. 61, 01187 Dresden, Germany*
[3]*Technische Universität Dresden, Institut für Fertigungstechnik, George-Baehr-Str. 3c, 01069 Dresden, Germany*
[4]*PROBIEN-CONICET, Dto. de Electrotecnia, Universidad Nacional del Comahue, Buenos Aires 1400, Neuquén 8300, Argentina*
[5]*Fraunhofer-Institut für Werkstoff- und Strahltechnik (IWS), Winterbergstraße 28, 01277 Dresden, Germany*
[*]*milan.kovacic@fe.uni-lj.si*

Abstract: Hierarchical textures (combining 2D periodic large and small micro textures) as an external outcoupling solution for OLEDs have been researched, both experimentally and by optical simulations. For the case of a red bottom emitting OLED, different hierarchical textures were fabricated using laser-based methods and a replication step and applied to the OLED substrate, resulting in an increased light outcoupling. Laboratory-size OLED devices with applied textured foils show a smaller increase in efficiency compared to the final large area devices. The results show that the full exploitation of textured foils in laboratory-size samples is mainly limited by the lateral size of the thin film stack area and by limited light collection area of the measuring equipment. Modeling and simulations are used to further evaluate the full prospective of hierarchical textures in large area OLED devices. Optimization of hierarchical textures is done by simultaneously changing the aspect ratios of the small and large textures and a potential of 57% improvement in *EQE* compared to devices without applied textures is predicted by simulations. Optimized hierarchical textures show similar outcoupling efficiencies compared to optimized single textures, while on the other hand hierarchical textures require less pronounced features, lower aspect ratios, compared to single textures to achieve the same efficiencies. Hierarchical textures also help in eliminating flat parts that limit outcoupling efficiency. Finally, the limiting factors that prevent higher outcoupling are addressed. We show that the dominant factor is non-ideal reflection from the organic thin film stack due to parasitic absorption. In addition, possible ways to further increase the outcoupling from a thick substrate are indicated.

1. Introduction

Organic light-emitting diodes (OLEDs) are commercially widespread in display technology and are also expanding into other areas such as wearable electronics, healthcare applications and lighting [1–5]. OLEDs present an opportunity for low-cost, high quality general lighting solutions with homogenous emission over large areas and superior color quality and high efficiency. As OLEDs can be made on rigid or flexible substrates and can be made transparent for usage on windows, they offer a wide variety of options in design and architecture.

OLEDs efficiency potential lies in highly optimized materials and structures, exhibiting internal efficiencies (electron to photon conversion) up to 100% for devices based on phosphorescence, thermally activated delayed fluorescence emission and for new emerging concepts like hyper

fluorescence [6–8]. On the other hand, relatively poor light outcoupling remains one of the main limiting factors in OLED overall performance, regardless the vast progress in internal efficiency of devices. Optical losses in OLEDs are mainly a consequence of total internal reflection (TIR), originating from difference in refractive indices of used materials. Additional optical losses are related to parasitic absorption of light in layers and non-ideal reflection at the rear side. Other optical losses are due to coupling of light to surface plasmon polaritons (SPP) at metal surfaces. Light generation occurs inside optically thin organic layer stack, where individual layers have a higher refractive index values (n ~1.7–1.8) [9] than the substrate (usually glass or polymer foil (n ~1.5)) and external medium - air (n ~1). This difference results in increased reflection or even TIR for light travelling under large angles (over critical angles) at interface with refractive index contrast. Together, optical losses contribute between 70–80% of all OLED losses limiting efficiency up to 20–30% for common flat plane devices without any light outcoupling strategy [10,11].

Different solutions to improve the light outcoupling have been investigated, see for example recent published reviews [1,12,13]. Concepts, focusing on minimization of waveguided and SPP losses inside thin-film OLED stacks need to be designed and fabricated to be both optically effective and, most important, not to deteriorate electrical properties of the device. In contrast to internal structuring of OLED stack, optical solutions applied externally to the substrate aiming the substrate losses, avoid contact with sensitive organic layers and are thus advantageous from this point of view as there is no disturbance to the electrical performance of the device. One of these solutions is applying outcoupling foils to the substrate on the opposite side of the deposited organic layers. External outcoupling solutions can usually be fabricated easily and with low cost (e.g., UV-nano imprint lithography [14–16]). Although reaching only substrate TIR losses, these outcoupling solutions can still bring high improvements in outcoupling efficiency of OLED devices. Examples of external outcoupling solutions include different texturization, scattering films and micro-lens arrays [17–27]. Most of these outcoupling solutions work on principle of redirection of light and enabling transmittance of light over the critical angle and by this increasing probability for light being extracted.

In this paper we applied advanced optical modelling and simulations supported by experimental data to evaluate the potential of a low-cost, easy to fabricate textured foils with a special, so-called hierarchical texture as external light outcoupling structure. Hierarchical texture in our case means a combination of a large and a small microtextures. Multi-scaled texture concepts were already used as an external outcoupling solutions in OLEDs [28–30], with efficiencies above those of standard micro lens arrays (MLA) already achieved [28]. These published solutions rely on the combination of micro- and nano- scale textures, while here we focus on hierarchical textures with combination of microtextures that can be fabricated by two industrial-scalable laser-based methods. Namely, direct laser writing (DLW) [31,32] was used to produce the larger scale texture on steel plates, followed by a direct laser interference patterning (DLIP) step to engrave the texture with the smaller features [33,34]. Finally, these structured plates were used as stamps in a hot embossing process to transfer the texture to a soften polymer, enabling a low cost and high throughput light extraction solution [35]. Using modelling and simulations we study the potential of the hierarchical textures with different microtexture sizes with a realistic and with an idealized texture shape. First, we calibrate and validate the model to fabricated devices. We show the importance of considering finite lateral dimensions of laboratory-scale small-area devices and measuring equipment for collecting light in simulations of realistic devices. Then we extend the investigation of the potential of hierarchical microtextures to large devices, where device lateral dimensions become much larger (orders of magnitude larger) compared to the vertical ones. Optimization of large and small texture component in the hierarchical texture is carried out and benchmarked with a single component texture. Factors limiting efficiency of light outcoupling

related to external textures are investigated, main one being low reflectivity (parasitic absorption) of an OLED stack, in order to establish a pathway to further improvements in light extraction.

2. Experimental and modelling approach

2.1. OLED structure

Internally optimized p-i-n bottom emitting red OLED devices [36] were fabricated and considered in optical analysis. A schematic cross-section of the structure with functional layer names and corresponding thicknesses is presented in Fig. 1(a). Textured polymeric foil at the outer side - on top of the glass substrate is depicted schematically. Light generation by radiative recombination of electrons and holes takes place in the emission layer (EML). To ensure good supply of charge carriers (electrons and holes) and to increase recombination rate in EML, additional electron/hole transport layers (ETL, HTL) and electron/hole blocking layers (EBL, HBL) are included. Electrical contacts are provided by opaque silver (Ag) cathode and a transparent conductive oxide (TCO) as an anode - indium tin oxide (ITO) on glass substrate. Besides glass substrate, an encapsulation glass is considered at the cathode side. Fabrication details of the OLED samples and used materials can be found in [10].
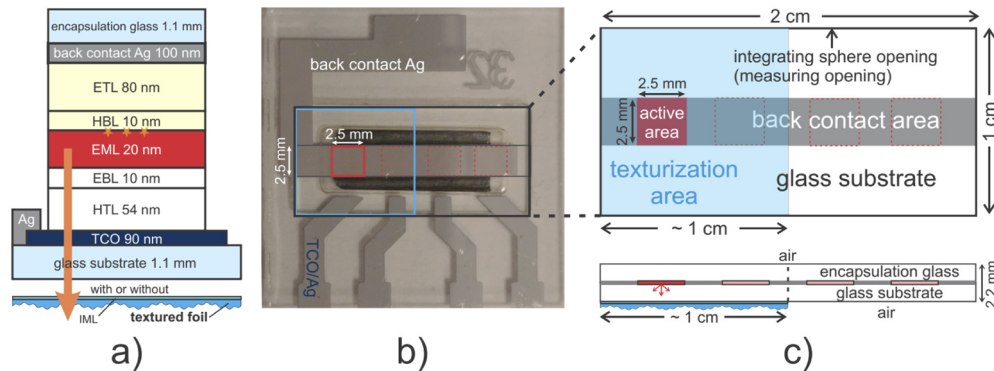

Fig. 1. a) Cross-section of a red bottom emitting OLED with corresponding layer thicknesses. External textured foil was applied to OLED device using index matching liquid (IML). b) Photograph of an actual lab-size OLED device used for measurements (front (bottom) side view - emission side), with marked active pixel area (red), texturization area (blue) and measuring opening area (black) c) Geometry as used in optical simulations corresponding to an actual OLED device – front and cross sectional side view.

The outcoupling texture was fabricated on a separate foil (for details on texture fabrication see chapter 2.2) and applied to the glass substrate using index matching liquid (IML, n ∼ 1.52). Due to very similar refractive indices of glass, IML and foil, in simulations the stack was considered as one thick layer. This simplification was done based on test simulations where all three layers have been considered separately, however negligible differences in simulation results have been observed with the simplified case.

Fabricated OLED samples (2.5×2.5 cm^2) as shown in Fig. 1(b) consist of four OLED pixels (an approximate pixel size of 2.5×2.5 mm^2) placed in a line. Each pixel is defined by the cross section of back contact Ag cathode and front ITO anode – one pixel is marked by a red rectangle in Fig. 1(b) and by red area in Fig. 1(c). OLEDs were measured by the integrating sphere using a sample holder (used to block side emission from the glass substrate) with an opening of 2×1 cm^2 as marked with a black rectangle. Textured foil with size 1×1 cm^2 is positioned above the active pixel as marked by blue color.

In the simulations we used a device geometry as sketched in Fig. 1(c). In our model we first limit simulation area (ray collection area) to the size of the sample holder opening. Active area, from which rays originate, was limited to the active pixel size and position. Thin-film stack of organic layers with Ag back contact (back contact area) is extending through entire holder opening as marked with gray color in Fig. 1(c), while the rest of the opening area (2×1 cm^2) has no additional thin film layers on the glass substrate. Supporting thin-film contacts lines (one is marked with TCO/Ag in Fig. 1(b)) that are used for supplying the current to the active pixel, and getter material (black part under the pixel area in Fig. 1(b)), cover only small part of the area, and show only small influence on results, thus they were discarded in the simulations.

Due to the relatively small area of the textured part of the foil in our samples ($\sim 1 \times 1$ cm^2), not covering entire measuring opening, we included in the model partial texturization area, as marked with semi-transparent blue color. Model also supports simulation of emission at the edge of applied foil, which can also contribute to the outcoupling – see an example in Supplement 1. Moreover, as it can be seen from the side view (Fig. 1(c) – bottom), we also included encapsulation glass at the rear side, since it can affect the amount of light collected in the measuring opening due to changed rear side reflection. Total thickness of glass substrate and encapsulation glass was 2.2 mm, as measured using a caliper.

2.2. Hierarchical textures

Textured polymer foils present a combination of large period (L) and small period (S) microtexture, that were replicated from a master stamp. Electropolished stainless steel plates (1.4301, Designblech GmbH, Germany) with a roughness of Sq = 15 nm and dimensions of 80 mm $\times$ 60 mm $\times$ 0.8 mm, were laser-patterned and then used as molds for hot embossing replication. Two laser-based manufacturing techniques were employed for texturing the metal master. First, direct laser writing (DLW) was used to pattern square arrays of craters with a period in the range of 30 μm to 70 μm (GF machining solutions P 600, Switzerland). This system consists of a nanosecond fiber laser emitting pulses with an energy of 0.1 mJ at a wavelength of 1064 nm and at a repetition rate of 30 kHz. The pulse duration was set to 200 ns and 500 pulses were shot at each position. The laser beam was scanned on the sample surface by using a high dynamic galvo-scanner system. The used f-theta lens with a focal distance of 254 mm yields a spot diameter in the focal plane of approximately 60 μm.

Afterwards, micropatterns were produced on the DLW-structured metal stamps using the direct laser interference patterning (DLIP) technique. Here, a solid state laser source (Neolase GmbH, Germany) emitting pulses at a wavelength of 532 nm with a pulse duration of 70 ps was used. For generating the DLIP pattern, the initial laser beam was split into four sub-beams by a diffractive optical element. Then the sub-beams were parallelized by a prism and recombined by a focal lens on the material surface. At the maxima positions of the periodic interference pattern, the material is ablated producing a dot-like texture on the sample. The spatial period of the dot-like patterns with four-beam interference can be fine-tuned by adjusting the overlapping angle [37]. In these experiments, the spatial period was set to 3.0 μm and 1, 5 and 10 pulses were applied on different flat and DLW-patterned steel plates. Further details about patterning hierarchical textures using these laser-based methods can be found elsewhere [38–41]. Afterwards, the laser-patterned plates were cleaned in an ultrasonic bath with isopropanol for 30 min and dried with compressed air. To avoid sticking of the polymer during the hot embossing, the stamps were coated with an anti-sticking layer. To this end, the structured masters were immersed in a solution of fluorophosphonic acid C6 (Teflon) and isopropanol (molar concentration of 2 mmol/L) for one hour. Afterwards, the samples were rinsed with isopropanol and annealed at 150 °C for 10 minutes.

Polyethylene terephthalate foils (PET, Pütz Folien GmbH, Germany) with a thickness of 200 μm were used as substrates for the hot embossing step. Before imprinting, the foils were cleaned

with pure ethanol and dried with compressed air. A temperature controlled hydraulic press (Paul-Otto Weber GmbH, Germany) was used to compress the laser-patterned stamps against the PET foils. The compression force was ramped from 0 to 200 kN within 30 s at room temperature. Considering the sample area of 4800 mm^2, a final pressure of 41.6 MPa was applied. In the next 5 min, the temperature was increased to 85 °C, then held for 10 min and decreased to 50 °C in the following 5 min. Then the pressure was released and the system was allowed to cool down to room temperature.

The fabricated textures were characterized by confocal microscopy (Sensofar S neox, Sensofar S.A., Spain) measurements. In Fig. 2(a), the topography of a selected hierarchical texture (patterned with a DLW period of 40 μm with 1 DLIP pulse) is presented. Profiles extracted from the topography data were used to calibrate the texture description in the model. The analysis of the texture shapes revealed that Gaussian functions can be used for fair description of the texture in the model (see Supplement 1). Besides the defined form (shape) each texture is characterized by its period (P), height (h) and aspect ratio ($AR = h / P$). Figure S3 of Supplement 1 summarizes the measured heights of the DLW and DLIP features on both stamps and imprints, showing a satisfactory replication of the textures' heights.
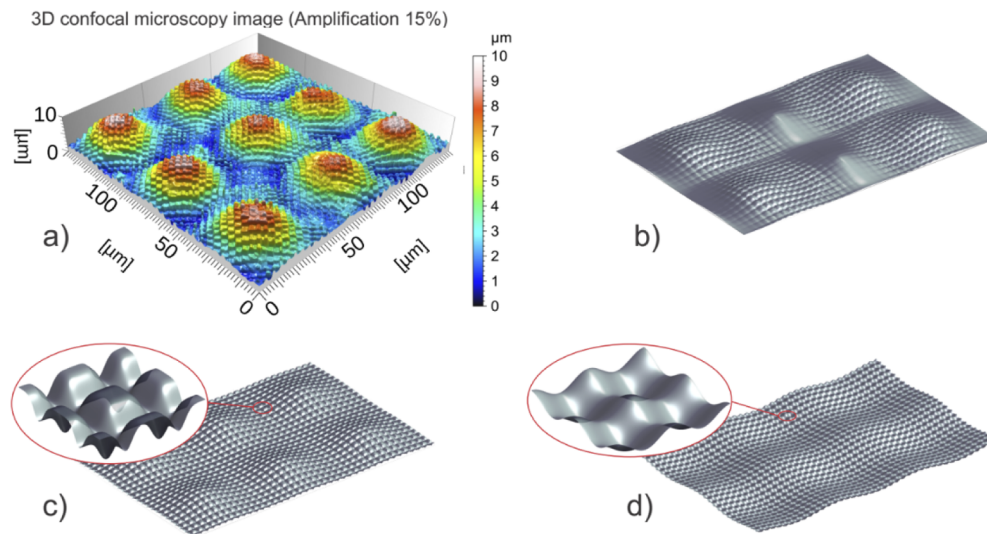

Fig. 2. a) Confocal microscopy image of a fabricated hierarchical texture H1 (large $P_L \sim$ 40 μm, $h_L = 4.2$ μm, $AR_L = 0.1$ and small $P_S = 3$ μm, $h_S = 1.3$ μm, $AR_S = 0.43$) texture as a combination of DLW and DLIP technique, respectively. b) hierarchical texture H1 as used in simulations, c) hierarchical texture with full coverage of both, small and large texture, d) a double sine-shaped hierarchical texture.

In Fig. 2(b) we show an example of the texture as used in simulations (fitted with Gaussian functions for S and L texture). Here, a partial coverage (∼50%) of the small texture on the larger one becomes evident. Partial coverage comes from DLIP fabrication process, exhibiting island like areas with more pronounced features and flat parts – see Supplement 1. Besides this more realistic case characterized by a partial covering, we took in simulations also textures featuring a full coverage of the small texture on the larger one, as can be seen in Fig. 2(c). As a consequence of the realistic shape of the texture, the fabricated L textures (with or without S textures) with $P > 50$ μm exhibit a kind of flattened areas, see Supplement 1), which were considered in simulations. To evaluate the full potential of hierarchical textures, in the simulations we consider also an idealized sine like hierarchical texture (sine like S and L texture), which does not have any flat area, as shown in Fig. 2(d).

Our simulation tests confirmed that for the used textures with feature sizes equal or above (≥ 3 μm) geometrical optics (ray tracing) can be applied without rigorous solving of electromagnetic waves in the microtextured region of the device. By combining different period and heights of both, S and L textures, we want to exploit this duality for improved light outcoupling.

2.3. Optical model

Analyzed OLED devices consist of an optically thin-film stack, where light needs to be modeled as waves, and optically thick substrate(s), where light needs to be treated as rays. This requires a combination of different modelling approaches. For analysis of such optical systems we developed a combined tool which was published in [27]. In the model, light emitting sources are represented by differently oriented dipole sources. Coherent propagation of light in the flat plane thin-film stack is described by transfer matrix formalism (TMM), considering wave nature of light, while for non-flat thin-film stack other approaches would be necessary [42]. Non-coherent light propagation in the optically thick substrate with or without micro-texture is modelled using a 3D ray tracing (RT) approach. Both methods (TMM and RT) are coupled by transformation of waves exiting thin-film stacks into rays by considering real part of the Poynting vectors with their intensities and directions. Rays are then traced through thick layers with flat or micro-textured interfaces. Reflected rays that are re-entering thin-film parts, are represented as waves with an arbitrary phase and are propagated using TMM again. This approach enables coupled optical simulations of entire OLED structure, including thin-film stack as well as thick microtextured substrate. Both approaches and final coupled model are described in detail in [20,27], with further details on TMM model [27] and RT model [43].

The developed model also enables the inclusion of different lateral limitations of realistic structures, such as limited light collection area, lateral size of thin-film structure (pixels, contacts geometry), limited texturization area and limited sample (substrate) size. All this is important to be considered when simulating small scale devices, as we already indicated in [44]. Additional upgrades to the model, also used for modelling in this contribution, include partial texture coverage and multiple thick layers (e.g., substrate and encapsulation).

We simulated OLED optical parameters, namely outcoupling efficiency ($\eta_{out}(\lambda)$) and Purcell factor ($F(\lambda)$). All other opto-electrical parameters (measured or simulated) used in this paper, can be gained using Eqs. (1)–(3):

$$EQE = \gamma \int_\lambda s_{el}(\lambda)\eta^*_{rad}(\lambda)\eta_{out}(\lambda)d\lambda \tag{1}$$

$$\eta^*_{rad}(\lambda) = \frac{\eta_{rad}F(\lambda)}{(1 - \eta_{rad} + \eta_{rad}F(\lambda))} \tag{2}$$

$$EQE(I_c) = \frac{e}{I_c hc} \int_\lambda \lambda\Phi(\lambda)d\lambda \tag{3}$$

where *EQE* is external quantum efficiency, γ is electrical efficiency, $s_{el}(\lambda)$ is normalized luminescence spectrum of emitting material, η^*_{rad} is effective radiative efficiency of the emitter, defined with the intrinsic radiative efficiency of the emitter (η_{rad}), Φ is spectral radiant flux, e is elementary charge, h is Planck constant, c is speed of light in vacuum and I_c is input electrical current. Presented parameters, in particular electrical efficiency, $\gamma = 1$, anisotropy, $a = 0.24$, radiative efficiency $\eta_{rad} = 0.82$ and normalized spectrum ($s_{el}(\lambda)$), are assumed from internal sources and literature [10] and correspond well to the analyzed flat device. All parameters are kept constant for all simulations, unless specified otherwise.

3. Results

3.1. Model validation

Before we used the model as a tool for analysis of optical situation in the device and for further optimization of the textures to improve the outcoupling performance, we validated our model on the fabricated samples. The validation of the model was carried out on the lab-size bottom-emitting red OLED device with different textured foils applied to the glass substrate, as described in the previous section. In the following simulation cases we consider all lateral limitations of the device and the measurement system as described above, unless noted differently. Figure 3(left) presents measured and simulated *EQE*s. Results are shown for five different outcoupling foils applied, starting with non-textured flat (F) foil, followed by 2 foils, each textured with single small (S, $P_S = 3$ μm, $h_S = 2.2$ μm, $AR_S = 0.73$), or large (L, $P_L = 39$ μm, $h_L = 4.2$ μm, $AR_L = 0.1$) sized texture and two foils textured with hierarchical (H1, $P_L = 39$ μm, $h_L = 3.6$ μm, $AR_L = 0.09$ and $P_S = 3$ μm, $h_S = 0.6$ μm, $AR_S = 0.2$ and H2, $P_L = 39$ μm, $h_L = 4.2$ μm, $AR_L = 0.1$ and $P_S = 3$ μm, $h_S = 1.3$ μm, $AR_S = 0.4$) textures – see Fig. 3(right). In all the cases the internal OLED structure is kept the same, in experiments and in simulations.
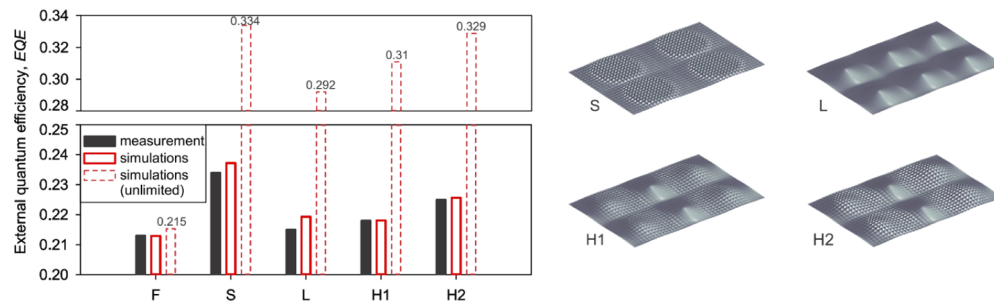

Fig. 3. Left: Comparison between measured (full black bars) and simulated (empty red bars) *EQE*s for OLEDs with different textures applied. Added (dashed empty red bars) are *EQE*s (simulated) as predicted for large area devices, where lateral limitations are excluded. Right: Representation of textures and corresponding denotations: S – small texture ($P_S = 3$ μm, $h_S = 2.2$ μm, $AR_S = 0.73$), L – large texture ($P_L = 39$ μm, $h_L = 4.2$ μm, $AR_L = 0.1$), H1 – hierarchical texture 1 ($P_L = 39$ μm, $h_L = 3.6$ μm, $AR_L = 0.09$ and $P_S = 3$ μm, $h_S = 0.6$ μm, $AR_S = 0.2$), H2 – hierarchical texture 2 ($P_L = 39$ μm, $h_L = 4.2$ μm, $AR_L = 0.1$ and $P_S = 3$ μm, $h_S = 1.3$ μm, $AR_S = 0.4$), whereas denotation F in the left figure corresponds to a non-textured flat-plane device.

In Fig. 3 measured results should be compared with the red full-line bars. These bars correspond to simulations considering all lateral geometries of the realistic devices. Good matching between measured and simulated results can be observed in all cases corresponding to various foil texturizations. Small differences between simulations and measurements can be attributed to the idealized texture and structure used in simulations, resulting in higher *EQE*. For additional comparison between measurements and simulations of single textures (both S and L) see Supplement 1. By comparing the effects of different texturizations (measured and well reproduced by simulation), the results show that applying textured foil results in an increased *EQE* that is attributed to the improved light outcoupling, as all other parameters of the device remained unchanged.

Among the selected single textures, both small (S) and large (L) textures show an increase in *EQE*. Especially S texture, with more pronounced features (larger $AR = 0.73$) exhibits higher improvement in *EQE*, while for selected L texture (less pronounced features, smaller $AR = 0.1$) only minimum increase is observed, coinciding with findings shown later in this paper.

Comparably to the selected single textures, both presented hierarchical textures H1 and H2 show an increase in *EQE*. For H1 texture with small features (small *AR* for both L and S texture) only minimum increase is observed in both simulations and measurements. For H2 texture with larger features (especially large *AR* of S texture), the increase in *EQE* is larger. As large textures have in all cases similarly low *AR*, the difference in outcoupling of presented hierarchical textures is mainly dominated by small textures exhibiting higher *AR*s. Presented hierarchical textures in this case show inferior results compared to selected S texture but superior to the L texture.

In the next step, we excluded lateral geometry limitations in the simulations, approaching the realistic situation of commercial size OLED devices. Results of these simulations are added in Fig. 3(left), presented by dashed red bars. While for flat device, only minimal difference can be observed between small and large size device, much larger changes showing highly increased *EQE* for unlimited devices can be observed for textured devices. The effect has already been addressed in our previous publication [20,44].

Production-scale OLED devices are mostly considered to be homogeneous large area devices, with lateral dimensions exceeding 10 cm^2, where edge effects have only a minor role. As there is no sample holder present, all light exiting substrate is extracted. Moreover, pixelated design and partial coverage of textures is not expected to be presented in final large area devices. Thus, to evaluate full potential of hierarchical textures on large area devices, we simulate and perform further optimization on homogeneous, large area (unlimited) devices only.

However, to indicate main restrictions which limit the potential of textured foils in small area devices we performed additional simulations where we systematically eliminated individual lateral constraints of the devices, towards final unlimited devices.

In Fig. 4 (left) we show measured spectral radiant flux ($\phi(\lambda)$ at 15 mA/cm^2 of applied electrical current density of an OLED without texturization and the same OLED with applied hierarchical texture (H2 – as seen in Fig. 3 (right)) using black and red symbols, respectively. Relatively high applied current density was used to increase the intensity of light and, thus, reduce measurements errors. Increase from optimal (highest measured *EQE*) driving current from ∼ 2 mA/cm^2 to 15 mA/cm^2 resulted in slightly reduced *EQE* (roll off), from value of 21.3% to 19.4% for the measured device. The reduction is attributed to the reduced internal efficiency, which was decreased by 9% in these simulations.
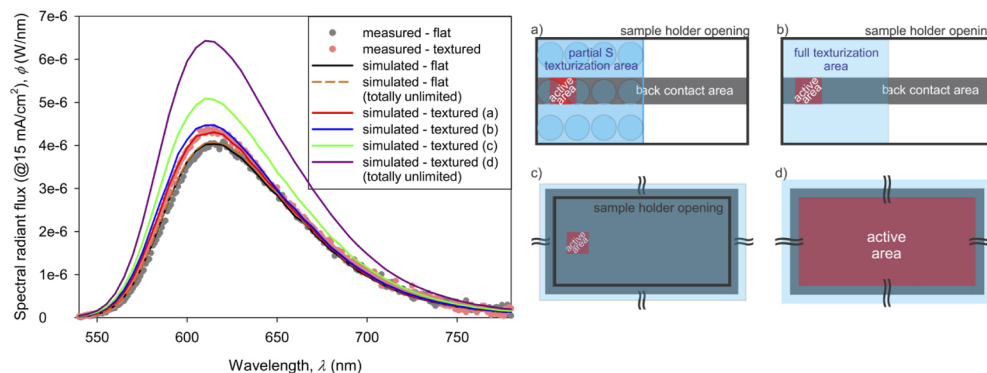

Fig. 4. Left: Measured $\phi(\lambda)$ (circles) for flat and H1 textured device, compared to simulated $\phi(\lambda)$, considering different levels of lateral limitations as presented on the Right part of the figure: a) limitations as in realistic measurement setup (partial texture coverage, limited measuring area, limited back contact area), b) the same limitations as in a) but with full coverage of large texture with small one, c) same structure as in b), but with unlimited texture area and unlimited back contact area, d) same ac c) but fully unlimited.

In Fig. 4 (left) we added to the measured $\phi(\lambda)$ curves (symbols), simulated ones (lines) corresponding to considered different lateral size limitations. Good spectral matching between simulations and measurements, both for flat and textured foil, can be observed for simulations where all mentioned lateral limitations as present in realistic device were considered (full black and red curves). Full blue curve corresponds to case b) in Fig. 4 (right), where instead of partial coverage of small textures on top of large ones (e.g., Fig. 1(b)) we introduce full coverage of small textures on top of large ones (e.g., Fig. 1(c)). Full green line corresponds to case c) in Fig. 4 (right), where we laterally extend thin-film stack including back contact and texturization over entire surface, as is the case in the large area devices. We still leave limited holder opening and limit light emission inside the measurement system. Final violet curve corresponds to the case d) in Fig. 4 (right), where we also remove holder limitation and extend emission area over entire surface, approaching final large area devices.

By comparing all these simulation curves one can observe significant increase in $\phi(\lambda)$ for the textured devices if starting with fully limited small area device and ending with laterally unlimited device. Presented results reveals that full exploitation of textured foils is mainly linked to largening the lateral size of the thin-film stack area (Fig. 4(c)) and the measuring opening (Fig. 4(d)). In case of a flat device the variation of lateral limitations affects the $\phi(\lambda)$ negligibly as can be seen from $\phi(\lambda)$ for fully limited (full black line) and fully unlimited (dashed orange line) device with almost insignificant differences.

3.2. Optimization of textures

In previous section we demonstrated a good agreement between simulated and measured characteristics of selected OLED samples. Based on this, we consider our model to be a reliable tool for investigation and prediction of improvements in OLED optical characteristics related to different hierarchical textures. From here on we consider homogeneous large area OLEDs with homogeneous coverage of large texture with small ones in case of hierarchical textures (Fig. 1(c, d)). To evaluate full potential of hierarchical textures we performed a series of simulations, testing different combinations of small and large textures by individually changing AR of each one. We take into consideration combination of large textures with periods ranging from $P_L = 30–69\ \mu m$ and small textures with a single period $P_S = 3\ \mu m$, that are feasible to produce with the presented laser-based methods. In Fig. 5(a) and 5(b) we show simulated EQE as a function of aspect ratio, AR_L, of the large texture for $P_L = 30\ \mu m$ and $P_L = 69\ \mu m$, respectively. Besides the AR_L the corresponding height of the L texture is included in the upper abscise axis. Different curves in the graphs corresponds to different AR_S (and h_S) of the small textures applied in hierarchical ones. Thus, figures present a collection of results where AR_S and AR_L in hierarchical textures were changed in the range from 0 to 1.
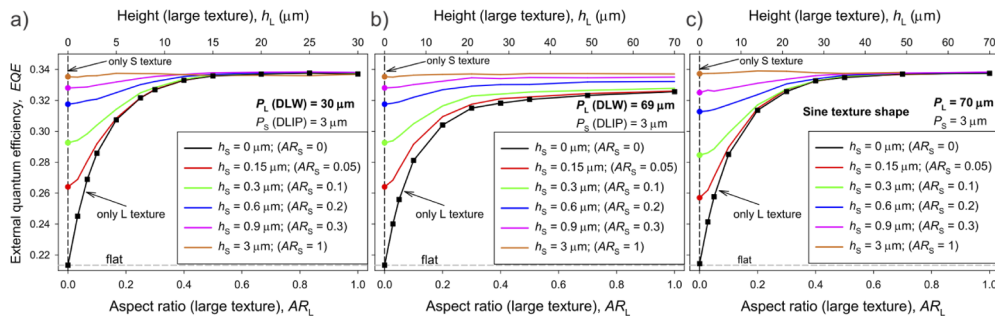

Fig. 5. *EQE* as simulated for different combinations of small and large gaussian-shaped textures in hierarchical combination, a) for $P_L = 30\ \mu m$ and $P_S = 3\ \mu m$, b) for $P_L = 69\ \mu m$ and $P_S = 3\ \mu m$ and c) with the period sizes as in b) but for sine-shaped hierarchical texture.

In both cases (Fig. 5(a) and 5(b)), one can observe an increase in *EQE* by increasing AR_S for small AR_L, as well as an increase in *EQE* by increasing AR_L for small AR_S. When one of the textures $AR_{(S \text{ or } L)}$ reaches high values (above 0.5), adding a secondary texture $AR_{(L \text{ or } S)}$, does not result in further change of *EQE*. For high AR_S or AR_L or combination of both, saturation in *EQE* of 33.7% is achieved.

Results for the case with $P_L = 30$ μm (Fig. 5(a)) show that texturization improves *EQE* from ~21.3% (device without texturization) up to ~33.7% for best textures presenting relative 57% improvement. In the graph black symbols represent device with L texture only and color symbols represent device with S texture only. Results show that increasing *AR* up to a ~0.5, of a single textures (L or S) results in an increasing *EQE* with a saturation level of ~ 33.7%. Further increase of *AR*, above 0.5, exhibits only minimal change in *EQE* for both S or L individual texture. Moreover, results show that even best hierarchical textures do not significantly exceed *EQE* of single L or S optimized texture (high enough *AR*).

Similar results as for $P_L = 30$ μm, can be observed also for $P_L = 69$ μm. However, a significant difference is for high AR_L where we do not reach the level of *EQE* as achieved with high AR_S textures. Simulations showed that the reason for this are flat parts of large texture, as a consequence of its shape (for details see Supplement 1). In this case, S textures cover flat parts of the L texture, resulting in a hierarchical texture without any flat parts. Here hierarchical textures enable increased outcoupling, above the one achievable with only single texture exhibiting flat parts.

In further investigation we introduce an idealized shape of the texture, i.e. 2D sinus-like texture (Fig. 2(d)). This texture does not contain flat parts even for larger values of P_L. Results of simulations of sine-like hierarchical textures are presented in Fig. 5(c). Here, one can observe similar trend of saturation like observed for L texture $P_L = 30$ μm in Fig. 5(a). Additional observation is that highest *EQE*s achieved for sine-like hierarchical textures are similar to the ones for optimized realistic hierarchical texture described by gaussian functions (*EQE* ~ 33.7%).

4. Discussion

From results in Fig. 5, where black rectangular and color circular symbols presenting only L and only S texture, respectively, we can observe that very high *EQE* can be achieved not only by gaussian-shaped hierarchical textures, but also with optimized single textures, both L and S (as well as with sine-like texture). Hierarchical textures in this respect do not show further improvement in overall *EQE* over optimized single ones, however, they do offer possibility for improved *EQE* for realistic L textures produced by DLW with flat areas, where we can use small textures to eliminate flat parts and thus improve *EQE*. Additionally, hierarchical textures can help to improve outcoupling if we are limited in fabrication with textures having small *AR*s, in this case a combination of two textures, S and L with smaller *AR*s we can reach *EQE*s of single texture with high *AR*. For example, for hierarchical texture with $AR_L = 0.3$ & $AR_S = 0.3$ we can achieve similarly high *EQE* as with single texture (L or S) of $AR = 0.5$.

To evaluate optical performance of either single or hierarchical textures in a more generalized way we further research factors limiting outcoupling improvements. We start by evaluating transmittance of a single interface substrate/air with different textures applied to it. In Fig. 6 we show simulated transmittance, *T*, of the interface considering ½ transversal electric (TE)+ ½ transversal magnetic (TM) polarization of light applied under different incident angles. Similar situation occurs in OLED, where light is propagating under different incident angles as indicated by simulated angular intensity distribution (AID) of light after entering the substrate (dashed curve in Fig. 6). Transmittance of the interface is shown for the flat interface, interface with texture, exhibiting poor outcoupling ability (sine-like texture with low $AR = 0.3$ ($P = 69$ μm)), and for two textures with identified good outcoupling ability (sine-like texture with high AR = 0.7 (P=69 μm)) and hierarchical texture ($P_L = 69$ μm, $P_S = 3$ μm) with ($AR_L = 0.7$, $AR_S = 0.3$)). For

flat interface we can observe high transmittance of light for angles smaller than critical angle, while for higher angles no light is extracted due to TIR, leaving large amount of light waveguided in the device. For the texture with poor outcoupling ability (green line) we can also observe high transmittance for smaller angles, afterwards T starts to fall considerably and for higher angles (~70° in this case) transmittance is reduced to practically zero. On the other hand, for textures with good outcoupling ability (blue for single scale texture, red for a hierarchical one), much smaller T is observed for smaller angles, while for large angles (especially over critical angle) outcoupling is increased. For even higher angles above 70°, transmittance falls considerably but not to zero, as with flat and poor outcoupling textures. Comparing transmittance between good single and good hierarchical texture show similar trends, with only small differences between them. Results indicate that outcoupling texture enables transmission for larger angles above critical angle, which appears to be very important, while for smaller angles transmittance is even reduced, but does not have significant impact. Non-zero transmittance for angles above the critical angle is achieved with optimized single or hierarchical texture, while no improvement in T over single texture is observed by hierarchical textures. To see how these findings correspond to actual measured results, T simulations were done for the case with real fabricated textures (see textures in Fig. 3 – right). In Fig. 6(b) we can, similar to results with sine textures shown in Fig. 6(a), observe that adding a texture at the substrate/air interface results in decrease of T for angles below and increase of T for angles above critical angle. Moreover, textures enabling higher T for angles above critical angle – Fig. 6(b), match directly to increase in measured *EQE* of OLED device (Fig. 3) with the applied corresponding textures. Fabricated texture with highest T for angles above critical angle was S texture ($P = 3$ μm, $h = 2.2$ μm, AR $= 0.7$), that also results in highest *EQE* when used as outcoupling texture in OLED device. Fairly lower T for higher angles of fabricated S texture compared to sine texture (with similar AR) result from non-homogeneous texture surface, exhibiting flatter parts, as can be seen in Fig. 3 – right, which in combination with lateral limitations as described in previous sections, results in lower *EQE* as achievable in optimized case. On the other hand, for lower angles we can observe higher T for fabricated textures while this, as discussed above, has only minimal impact on increased outcoupling.
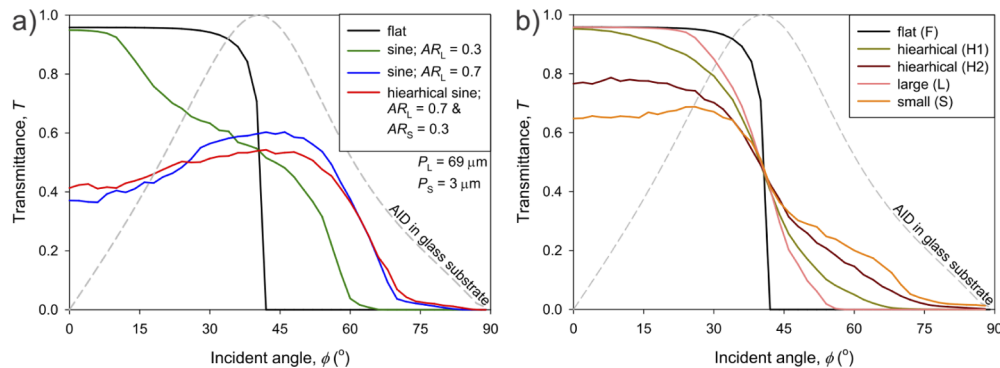

Fig. 6. Simulated angular dependent transmittance of glass/textured foil/air structure for different incident angles and selected foil textures. Normalized angular intensity distribution (AID) of monochromatic ($\lambda = 610$ nm) light as present in the glass substrate before the first pass through the glass/textured foil/air structure is added to both graphs. a) T for sine shaped textures b) T for realistic fabricated textures (for textures see Fig. 3)

Furthermore, we investigate how the outcoupling process is constructed by each single pass of the texture, as we know that the light is propagating in forward and backward directions throughout the structure due to multiple reflection-transmission process at interfaces and thus, hits the glass/air interface more times. In this special kind of simulations, we take the light

in glass with its actual AID as emitted from the thin-film stack, excluding back reflections at the substrate/air interface (obtained by simulations considering infinite substrate). Light with such distribution is sent through the flat or textured interface and the total amount of light being transmitted and reflected at the substrate/air interface is monitored. All the reflected light at the substrate/air interface (with the newly calculated AID and new polarization share, both dependent on the texture applied) is in this simulation first artificially reduced for selected constant factors, to mimic all the parasitic optical losses inside the device for the back reflected light at substrate/air interface. This constant reduction factor can be also assigned to reflection factor of entire thin-film OLED stack, including back metal contact (R_{TF}). Next this light is directed to the substrate/air interface for the next pass. With such analysis we decouple contributions to outcoupling related to different subsequent passes of light and indicate the role of R_{TF} on the final transmitted power. Results of these simulations are presented in Fig. 7(a) for different R_{TF} stack values. Formation of the final normalized transmitted power through the substrate/air interface is shown step by step. Normalized power of the first pass of light is surprisingly almost independent of the interface textures. In the first pass a very similar amount of light ~45% is transmitted from substrate to air no matter the texture or the lack of it (flat interface). Furthermore, for textured interface increase in total transmitted power increases with number of passes, however a saturation is observed after around 10 passes for all analyzed textures and R_{TF} values. Difference between good and poor outcoupling texture can be observed both in rate of increase as well as in final normalized transmitted power. It can be observed that the final transmitted power is pre-defined by the R_{TF} stack. Simulations revealed that different values of R_{TF} stack do affect the transmitted power of the structures with textured substrate/air interface significantly. Added in Fig. 7(a) is the ideal case with $R_{TF} = 1$, where we can observe an even faster rise in transmitted power with each texture pass and final value approaching 100% after 10 passes. If we assume that the R_{TF} stack is mainly defined by back metal reflector the observation in Fig. 7, regarding the saturation values from different R_{TF} stack is in accordance with results reported in [18].
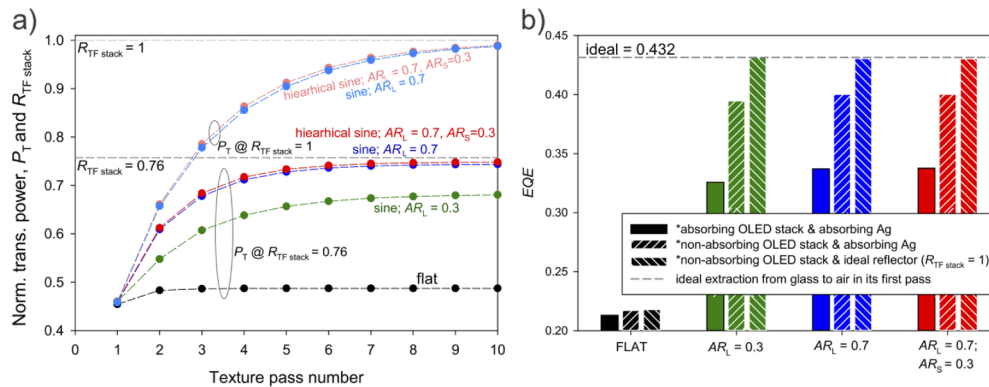

Fig. 7. a) Normalized transmission power of light in the air shown sequentially as a function of texture pass number for a simplified structure with a defined reflection of the OLED + back contact stack, R_{TF}, dashed lines are used as a guide for the eye b) Simulated *EQE* of the OLED with different textures and back reflection properties. Left bars in the stacks represents *EQE* as achieved without any thin film stack modification, middle bars represent *EQE* as achieved by making thin-film stack non-absorptive (except Ag contact)*, and right bars represent *EQE* as achieved with ideal BR ($R_{TF} = 1$)* for each texture. Dashed grey line represents *EQE* as achieved by ideal extraction of light from glass substrate. *valid only for rays reentering thin-film stack (reflected from glass/air interface), while emission into glass from thin-film stack was calculated with fully realistic stack.

From these decoupled simulations it can be observed that further potential of outcoupling, related to different textures with non-zero transmitted power for large incident angles is in tight connection with high R_{TF} stack. R_{TF} stack can be improved by improving reflection of back reflector and minimizing parasitic optical losses in OLED stack.

To evaluate this potential related to the realistic device (considering realistic thin-film stack in these simulations) we test three different scenarios in final simulations. The aim is to show the potential of different textures in relation to optical losses in thin-film stack. Here R_{TF} factor is replaced by traveling of back reflected light throughout the thin-film OLED stack.

Here, realistic OLED thin film stack without modifications, is used to gain light in glass with its actual AID as emitted from the thin-film stack, excluding back reflections at the substrate/air interface (obtained by simulations considering infinite substrate) and is kept the same for all scenarios. Any modifications to the thin-film stack are considered only for light being reflected back from substrate/air interface.

The first scenario is an OLED stack including realistic parasitic absorption in OLED stack and losses related to realistic Ag reflector. In the second scenario we simulate OLED stack excluding parasitic absorption losses in OLED stack except in Ag layer. In the third scenario we consider an OLED stack without any losses when tracing reflected light from the glass/air interface (corresponds to the previous case R_{TF} stack = 1). Results of simulated *EQE*s for these scenarios are presented in Fig. 7(b). Simulation of an idealized case, where ideal transmission is applied to the substrate/air interface (already at the first light pass) is added for a reference (grey dashed line). Here light does not return into the OLED stack, thus, the three scenarios play no role on this result. However, for other mentioned simulated cases of the three scenarios results clearly indicate that by reducing losses in thin-film stack we can greatly enhance outcoupling potential of the textures.

Case with flat interface (no texture applied), presented with black columns in Fig. 7(b), shows only small increase in the final *EQE* for 3 different scenarios as mentioned above (from ~21.3%, 21.7% to 21.8%, respectively). Here, most light gets extracted in first transition already and only smaller amount of it can get extracted in next step as main part of light is reflected above critical angle and gets waveguided. For waveguided part, no matter the back reflection, this light remains lost, thus only minimal increase in *EQE* for different scenarios.

The case with poor outcoupling texture (sine like, $AR = 0.3$), represented by green columns in Fig. 7(b) exhibits increase in *EQE* from scenario 1 to scenario 3 from 32.6%, 39.5% to 43.1%, respectively. Here due to multiple reflections from thin-film OLED stack, reduction of reflection losses results in higher outcoupling as less light is lost at each reflection and thus more reflections are possible before light gets reabsorbed, increasing probability for extraction. Interestingly for ideal reflection – scenario 3, all light gets extracted from the glass substrate, even though the texture is not optimal when using absorbing (with losses) thin-film stack.

Finally, for both good textures, single and hierarchical represented by blue and red columns, respectively in Fig. 7(b), we can observe almost identical increase in *EQE*s from scenario 1 to 3 (single: 33.7%, 40% and 43.1%; hierarchical: 33.8%, 40% and 43%). Compared to previous texture (green columns), here higher *EQE*s are achieved for scenarios 1 and 2, as for better textures more light is transmitted with each individual pass, resulting in less light being reflected and thus subjected to parasitic absorption losses of the OLED thin film stack. On the other hand, similar as with previous texture, highest possible *EQE* (~43%) is reached for scenario 3.

No significant difference between textures with poor or good (for absorbing thin-film stack) outcoupling efficiency is observable for ideal R_{TF}. Outcoupling solutions, that work on redirection of light (without flat parts), can be 100% efficient as long as there are no losses in the substrate and the thin film-stack as light gets eventually (multiple reflections) redirected and extracted. This is also the main reason for one of the common misconceptions for eliminating substrate losses, that all light reaching the substrate can get extracted from glass substrates by using texturization on

substrate/air interface, but this would only be true if $R_{\text{TF}} = 1$ as shown here. In reality, reflectivity of an OLED stack is lower than 1, enabling only partial extraction of light from the substrate when using different outcoupling solutions. Reduction of parasitic absorption losses in thin-film stack shows more importance than further optimization of the texture.

5. Conclusion

Hierarchical textures, fabricated with a combination of two laser techniques, i.e., DLIP and DLW, and one replication step, were investigated and used to enhance outcoupling of light from substrate to air for the case of red bottom emitting OLED devices. Optical modelling was utilized to analyze the effect in small and large size OLED devices.

Measurement of OLED devices, with and without attached hierarchical textures, was done on small laboratory-size samples. Attached hierarchical textures resulted in improved efficiency of these laboratory-size OLEDs. Good matching between measured and simulated results was achieved only when various lateral limitations and specifics of lab-size samples were considered in the optical model. These include limited holder opening, pixelated design and partial texture coverage, as well as double thickness of glass substrate and encapsulation. Moreover, small lab-size samples with attached outcoupling foils, show much lower efficiency compared to final large area devices. Evaluation of these differences was done using simulations by systematically removing small sample limitations, until reaching large area device, revealing main limiting factors of small lab-size samples to be limited holder opening area, pixelated design of back contact and partial texturization coverage.

Using modelling and simulations we further investigated the potential of hierarchical textures of large area OLED devices. Hierarchical textures with optimal combination of small and large textures, exhibiting high enough combined *AR* (high enough *AR* of both small and large textures), show relatively high *EQE* of 33.7% which is more than 57% improvement in comparison to flat (*EQE* = 21.3%). However, a comparison with optimized single textures with high enough *AR* > 0.5, revealed that there is almost no improvement in *EQE* of hierarchical textures over optimized single textures. However, hierarchical textures are better-suited for light outcoupling, when single scale textures with high aspect ratios (*AR* > 0.5) are difficult to fabricate, which is the case for DLW or for DLIP structures with small periods (*P* < 1.5 μm). Therefore, by combining a small and a large texture both with intermediate *AR* (< 0.3) it is possible to gain the same extraction efficiency as by a single texture with high *AR*. Moreover, hierarchical textures can also help in the extraction of light if the large texture includes some flat parts, which can be eliminated by hierarchical texturization.

Finally, a detailed optical analysis confirmed that outcoupling potential of texturization is governed by optical losses of the OLED stack. Simulation showed that the texture shape and size itself has only smaller effect, as long as it enables extraction of light beams under large angles and it sufficiently redirects rays to enhance probability for extraction in further passes of the texture. Thus, further improvements in light outcoupling can be obtained by improving back reflector, lowering parasitic losses in other layers or/and by applying more advanced solutions that would enable higher transmittance in less texture passes. Additionally, in this contribution we considered only micro-sized textures (geometrical optics), while another option would be to use for example nano texturization, that may enable higher transmittance already with smaller number of texture passes, thus reducing parasitic losses from OLED stack reflection. Moreover, final efficiency is also limited with the amount of light that reaches the substrate and is available for extraction with external textures, thus light extraction from the OLED organic stack to the substrate could bring further improvements.

Disclosures. The authors declare no conflicts of interest.

Data availability. Data underlying the results presented in this paper are not publicly available at this time but may be obtained from the authors upon reasonable request.

Supplemental document. See Supplement 1 for supporting content.

References

1. J. Song, H. Lee, E. G. Jeong, K. C. Choi, and S. Yoo, "Organic Light-Emitting Diodes: Pushing Toward the Limits and Beyond," Adv. Mater. **32**(35), 1907539 (2020).
2. R. Pode, "Organic light emitting diode devices: An energy efficient solid state lighting for applications," Renewable Sustainable Energy Rev. **133**, 110043 (2020).
3. Y. Chang and Z. Lu, "White Organic Light-Emitting Diodes for Solid-State Lighting," J. Disp. Technol. **9**(6), 459–468 (2013).
4. S. Reineke, M. Thomschke, B. Lüssem, and K. Leo, "White organic light-emitting diodes: Status and perspective," Rev. Mod. Phys. **85**(3), 1245–1293 (2013).
5. Y. Yin, M. U. Ali, W. Xie, H. Yang, and H. Meng, "Evolution of white organic light-emitting devices: from academic research to lighting and display applications," Mater. Chem. Front. **3**(6), 970–1031 (2019).
6. G. Hong, X. Gan, C. Leonhardt, Z. Zhang, J. Seibert, J. M. Busch, and S. Bräse, "A Brief History of OLEDs—Emitter Development and Industry Milestones," Advanced Materials n/a, 2005630 (n.d.).
7. L. Xiao, S.-J. Su, Y. Agata, H. Lan, and J. Kido, "Nearly 100% Internal Quantum Efficiency in an Organic Blue-Light Electrophosphorescent Device Using a Weak Electron Transporting Material with a Wide Energy Gap," Adv. Mater. **21**(12), 1271–1274 (2009).
8. C. Adachi, G. Xie, S. Reineke, and E. Zysman-Colman, "Editorial: Recent Advances in Thermally Activated Delayed Fluorescence Materials," Front. Chem. 8, (2020).
9. M.-H. Lu and J. C. Sturm, "Optimization of external coupling and light emission in organic light-emitting devices: modeling and experiment," J. Appl. Phys. **91**(2), 595–604 (2002).
10. R. Meerheim, M. Furno, S. Hofmann, B. Lüssem, and K. Leo, "Quantification of energy loss mechanisms in organic light-emitting diodes," Appl. Phys. Lett. **97**(25), 253305 (2010).
11. S. R. Forrest, D. D. C. Bradley, and M. E. Thompson, "Measuring the Efficiency of Organic Light-Emitting Devices," Adv. Mater. **15**(13), 1043–1048 (2003).
12. M. C. Gather and S. Reineke, "Recent advances in light outcoupling from white organic light-emitting diodes," J. Photon. Energy **5**(1), 057607 (2015).
13. A. Salehi, X. Fu, D.-H. Shin, and F. So, "Recent Advances in OLED Optical Design," Adv. Funct. Mater. **29**(15), 1808803 (2019).
14. J. Escarré, K. Söderström, C. Battaglia, F.-J. Haug, and C. Ballif, "High fidelity transfer of nanometric random textures by UV embossing for thin film solar cells applications," Sol. Energy Mater. Sol. Cells **95**(3), 881–886 (2011).
15. M. Meier, U. W. Paetzold, M. Prömpers, T. Merdzhanova, R. Carius, and A. Gordijn, "UV nanoimprint for the replication of etched ZnO:Al textures applied in thin-film silicon solar cells," Prog. Photovolt: Res. Appl. **22**(12), 1226–1236 (2014).
16. M. Jošt, S. Albrecht, L. Kegelmann, C. M. Wolff, F. Lang, B. Lipovšek, J. Krč, L. Korte, D. Neher, B. Rech, and M. Topič, "Efficient Light Management by Textured Nanoimprinted Layers for Perovskite Solar Cells," ACS Photonics **4**(5), 1232–1239 (2017).
17. S. Möller and S. R. Forrest, "Improved light out-coupling in organic light emitting diodes employing ordered microlens arrays," J. Appl. Phys. **91**(5), 3324–3327 (2002).
18. H. Greiner, "Light Extraction from Organic Light Emitting Diode Substrates: Simulation and Experiment," Jpn. J. Appl. Phys. **46**(7A), 4125–4137 (2007).
19. H. Bae, J. S. Kim, and C. Hong, "Simulation for light extraction efficiency of OLEDs with spheroidal microlenses in hexagonal array," Opt. Commun. **415**, 168–176 (2018).
20. M. Kovačič, P.-A. Will, B. Lipovšek, M. Topič, S. Lenk, S. Reineke, and J. Krč, "Coupled Optical Modeling for Optimization of Organic Light-Emitting Diodes with External Outcoupling Structures," ACS Photonics **5**(2), 422–430 (2018).
21. G. Zhai, W. Zhu, L. Huang, C. Yi, and K. Ding, "Enhanced light extraction from green organic light-emitting diodes by attaching a high-haze random-bowls textured optical film," J. Phys. D: Appl. Phys. **53**(43), 435101 (2020).
22. J.-G. Zhou, X.-C. Hua, C.-C. Huang, Q. Sun, and M.-K. Fung, "Ideal microlens array based on polystyrene microspheres for light extraction in organic light-emitting diodes," Org. Electron. **69**, 348–353 (2019).
23. T. T. K. Tu, J. W. Han, D. W. Kim, Y. T. Jeong, Y. S. Gal, L. G. Bach, Y. H. Kim, and K. T. Lim, "Enhancement of Light Extraction from Organic Light-Emitting Diodes by SiO2 Nanoparticle-Embedded Phase Separated PAA/PI Polymer Blends," Mol. Cryst. Liq. Cryst. **686**(1), 55–62 (2019).

24. J.-H. Yen, Y.-J. Wang, C.-A. Hsieh, Y.-C. Chen, and L.-Y. Chen, "Enhanced light extraction from organic light-emitting devices through non-covalent or covalent polyimide–silica light scattering hybrid films," J. Mater. Chem. C **8**(12), 4102–4111 (2020).

25. A. Gasonoo, Y.-S. Lee, J.-H. Yoon, B.-S. Sung, Y. Choi, J. Lee, and J.-H. Lee, "Outcoupling efficiency enhancement of a bottom-emitting OLED with a visible parylene film," Opt. Express **28**(18), 26724–26732 (2020).

26. J. Song, K.-H. Kim, E. Kim, C.-K. Moon, Y.-H. Kim, J.-J. Kim, and S. Yoo, "Lensfree OLEDs with over 50% external quantum efficiency via external scattering and horizontally oriented emitters," Nat. Commun. **9**(1), 3207 (2018).

27. M. Kovačič, P.-A. Will, B. Lipvošek, J. Krč, S. Lenk, S. Reineke, and M. Topič, "Combined optical model for micro-structured organic light emitting diodes," Informacije MIDEM **46**, 167–275 (2017).

28. Y. Han, C.-K. Moon, K. Kim, H. Lee, and J.-J. Kim, "Random organic nano-textured microstructures formed by photoexcitation for light extraction of blue OLEDs," Org. Electron. **87**, 105892 (2020).

29. K. Kim, K.-H. Han, Y.-D. Kim, D. Huh, Y. Han, H. Lee, and J.-J. Kim, "Dual pattern for enhancing light extraction efficiency of white organic light-emitting diodes," Org. Electron. **57**, 201–205 (2018).

30. J.-J. Kim, J. Lee, S.-P. Yang, H. G. Kim, H.-S. Kweon, S. Yoo, and K.-H. Jeong, "Biologically Inspired Organic Light-Emitting Diodes," Nano Lett. **16**(5), 2994–3000 (2016).

31. S. Hengsbach and A. D. Lantada, "Direct Laser Writing of Fractal Surfaces: Strategy to Design and Manufacture Textured Materials," Adv. Eng. Mater. **17**(2), 172–180 (2015).

32. V. D. Ta, A. Dunn, T. J. Wasley, J. Li, R. W. Kay, J. Stringer, P. J. Smith, E. Esenturk, C. Connaughton, and J. D. Shephard, "Laser textured superhydrophobic surfaces and their applications for homogeneous spot deposition," Appl. Surf. Sci. **365**, 153–159 (2016).

33. A. F. Lasagni, "Laser interference patterning methods: Possibilities for high-throughput fabrication of periodic surface patterns," Adv. Opt. Technol. **6**(3-4), 265–275 (2017).

34. D. W. Müller, T. Fox, P. G. Grützmacher, S. Suarez, and F. Mücklich, "Applying Ultrashort Pulsed Direct Laser Interference Patterning for Functional Surfaces," Sci. Rep. **10**(1), 3647 (2020).

35. A. Stellmacher, Y. Liu, M. Soldera, A. Rank, S. Reineke, and A. F. Lasagni, "Fast and cost effective fabrication of microlens arrays for enhancing light out-coupling of organic light-emitting diodes," Mater. Lett. **252**, 268–271 (2019).

36. P.-A. Will, M. Schmidt, K. Eckhardt, F. Wisser, S. Lenk, J. Grothe, S. Kaskel, and S. Reineke, "Efficiency of Light Outcoupling Structures in Organic Light-Emitting Diodes: 2D TiO2 Array as a Model System," Adv. Funct. Mater. **29**(20), 1901748 (2019).

37. B. Voisiat, "Flexible Microstructuring of Thin Films Using Multi-beam Interference Ablation with Ultrashort Lasers," JLMN **6**(3), 185–190 (2011).

38. F. Bouchard, M. Soldera, R. Baumann, and A. F. Lasagni, "Hierarchical Microtextures Embossed on PET from Laser-Patterned Stamps," Materials **14**(7), 1756 (2021).

39. M. Steger, "Fabrication of Hierarchical Structures by Direct Laser Writing and Multi-Beam-Interference," JLMN **8**(3), 210–215 (2013).

40. D. Huerta-Murillo, A. I. Aguilar-Morales, S. Alamri, J. T. Cardoso, R. Jagdheesh, A. F. Lasagni, and J. L. Ocaña, "Fabrication of multi-scale periodic surface structures on Ti-6Al-4V by direct laser writing and direct laser interference patterning for modified wettability applications," Optics and Lasers in Engineering **98**, 134–142 (2017).

41. S. Milles, M. Soldera, B. Voisiat, and A. F. Lasagni, "Fabrication of superhydrophobic and ice-repellent surfaces on pure aluminium using single and multiscaled periodic textures," Sci. Rep. **9**(1), 13944 (2019).

42. M. Kovačič, "Effect of Dipole Position and Orientation on Light Extraction for Red OLEDs on Periodically Corrugated Substrate - FEM Simulations Study," Informacije MIDEM **51**, 73–84 (2021).

43. B. Lipovšek, J. Krč, and M. Topič, "Optical model for thin-film photovoltaic devices with large surface textures at the front side," Informacije MIDEM **41**, 264–271 (2011).

44. M. Kovačič, P.-A. Will, B. Lipovšek, M. Topič, S. Lenk, S. Reineke, and J. Krč, "Improved light outcoupling of organic light-emitting diodes by combined optimization of thin layers and external textures," Proc. SPIE **10687**, 106870Z (2018).